HHS Public Access

Author manuscript

Nanomedicine. Author manuscript; available in PMC 2023 January 01.

Published in final edited form as:

Nanomedicine. 2022 January ; 39: 102459. doi:10.1016/j.nano.2021.102459.

Poly(2-oxazoline)-Magnetite NanoFerrogels: Magnetic Field Responsive Theranostic Platform for Cancer Drug Delivery and Imaging

Youngee Seo[a], **Lida Ghazanfari**[a], **Alyssa Master**[a], **Hemant M. Vishwasrao**[b], **Xiaomeng Wan**[a], **Marina Sokolsky-Papkov**[a,*], **Alexander V. Kabanov**[a,c,*]

[a.]Center for Nanotechnology in Drug Delivery, Division of Molecular Pharmaceutics, Eshelman School of Pharmacy, University of North Carolina at Chapel Hill, Chapel Hill, NC 27599-7362, United States

[b.]Center for Drug Delivery and Nanomedicine and Department of Pharmaceutical Sciences, College of Pharmacy, University of Nebraska Medical Center, Omaha, NE 68198-5830, United States

[c.]Laboratory of Chemical Design of Bionanomaterials, Faculty of Chemistry, M.V. Lomonosov Moscow State University, Moscow 119992, Russia

Abstract

Combining diagnosis and treatment approaches in one entity is the goal of theranostics for cancer therapy. Magnetic nanoparticles have been extensively used as contrast agents for nuclear magnetic resonance imaging as well as drug carriers and remote actuation agents. Poly(2-oxazoline)-based polymeric micelles which have been shown to efficiently solubilize hydrophobic drugs and drug combinations, have high loading capacity (above 40% w/w) for paclitaxel. In this study, we report the development of novel theranostic system, NanoFerrogels, which is designed to capitalize on the magnetic nanoparticle properties as imaging agents and the poly(2-oxazoline)-based micelles as drug loading compartment. We developed six formulations with magnetic nanoparticle content of 0.3~12 % (w/w), with the z-average sizes of 85–130 nm and ξ-potential of 2.7–28.3 mV. The release profiles of paclitaxel from NanoFerrogels were notably dependent on the degree of dopamine grafting on poly(2-oxazoline)-based micelles. Paclitaxel loaded NanoFerrogels showed efficacy against three breast cancer lines which was comparable to free paclitaxel. They also showed improved tumor and lymph node accumulation and signal

[*]**Corresponding authors:** M. Sokolsky-Papkov, A. V. Kabanov, Center for Nanotechnology in Drug Delivery, and Division of Molecular Pharmaceutics, Eshelman School of Pharmacy, University of North Carolina at Chapel Hill, Chapel Hill, NC 27599-7362, United States. Tel.: +1 919 537 3800; fax: +1 919 962 9922. kabanov@unc.edu (A.V. Kabanov); msokolsk@email.unc.edu (M. Sokolsky).

Author contribution

Author Contribution: Conceptualization, Y.S, M.S., and A.V.K; Methodology: Y.S., A.M., L.G., and X.W.; Software, Y.S., L.G., H.V., and X.W., Validation, Y.S., L.G., H.,V., and X.W.; Formal Analysis, Y.S., L.G., and X.W.; Investigation, Y.S., L.G., H.V., A.M., and X.W.; Resources, Y.S., L.G., A.M., and M.S.; Writing- Original Draft, Y.S., and L.G; Writing- Review and Editing, Y.S., L.G., M.S., and A.V.K.; Visualization, Y.S., and L.G.; Supervision, M.S., and A.V.K.; Project Administration, M.S., and A.V.K.; Funding Acquisition, M.S., and A.V.K. All authors have read and agreed to the published version of the manuscript.

reduction *in vivo* (2.7% in tumor; 8.5% in lymph node) compared to clinically approved imaging agent ferumoxytol (FERAHEME®) 24 hours after administration. NanoFerrogels responded to super-low frequency alternating current magnetic field (50 kA m^{-1}, 50 Hz) which accelerated drug release from paclitaxel-loaded NanoFerrogels or caused death of cells loaded with NanoFerrogels. These proof-of-concept experiments demonstrate that NanoFerrogels have potential as remotely actuated theranostic platform for cancer diagnosis and treatment.

Graphical Abstract

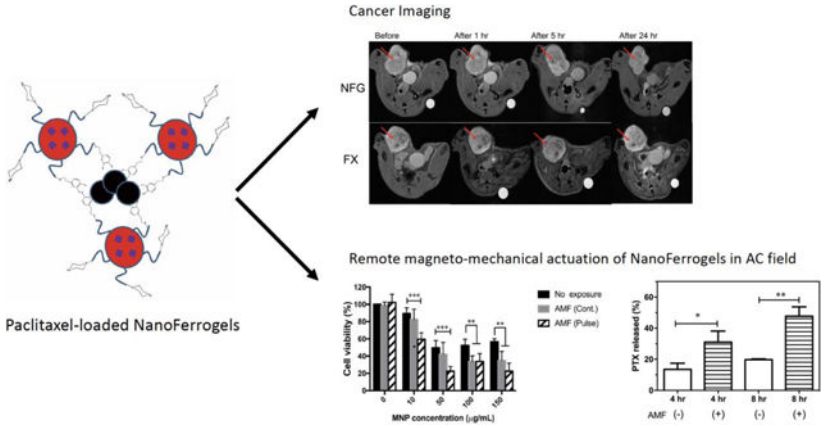

Novel Paclitaxel-loaded NanoFerrogels (PTX-NFGs) were developed with enhanced drug and magnetic nanoparticle loading capacity for drug delivery and imaging. Upon low frequency AC magnetic field exposure, PTX-NFGs triggered paclitaxel release and significant cytotoxic effect *in vitro*.

Keywords

magnetic nanoparticles; magneto-mechanical actuation; magnetic field-triggered release; Paclitaxel

1. Introduction

Most current applications of nanotechnology in cancer focus on development of separate systems for diagnosis and treatment of cancer, and it is necessary to shift the paradigm to combination of diagnosis and treatment in one single platform. Magnetic resonance imaging (MRI) has become one of the most used tools for non-invasive cancer diagnosis due to the high soft tissue contrast and spatial resolution [1,2]. Multifunctional all-in-one nanoparticle system can integrate diagnostic imaging component, and treatment [3,4]. Superparamagnetic iron oxide nanoparticles (MNPs) have different polymorphic forms, including magnetite (Fe_3O_4) and maghemite (γ-Fe_2O_3), and these two have shown promise as MRI contrast agents due to their good biocompatibility and feasibility of surface modification. Over the past decades, various MNPs were either clinically approved (i.e. Resovist®, GastroMARK®) or under clinical trials for cancer imaging [5]. Additional applications of MNPs, such as magnet targeted drug delivery, magnetic field-triggered drug release and gene expression

control, MNP-based hyperthermia [6,7] as well as magneto-mechanical actuation of MNPs [8] were reported. Contrary to magnetic hyperthermia, which utilizes a high frequency magnetic field to produce temperature increase in surrounding tissues, magneto-mechanical actuation induces mechanical motion of the MNPs and adjacent materials following exposure to super-low frequency AC magnetic field, without temperature increases [8]. In many theranostic studies active pharmaceutical ingredients (APIs) are chemically conjugated to polymer coated MNPs [9,10] which limits the API selection, the drug loading and the colloidal stability of nanoparticles [11,12]. Therefore, novel MNP-based formulations that can incorporate different APIs are needed for concurrent imaging, drug delivery and magneto-mechanical actuation.

Paclitaxel (PTX) is one of the most effective broad-spectrum anti-cancer agents approved for treatment variety of cancers, such as breast, non-small cell lung, ovarian and head and neck. Previously, we reported on poly(2-oxazoline) (POx) based polymeric micelles with very high drug loading capacity (LC) for PTX. POx-PTX micelles can be prepared with drug loading of up to 45 % w/w, which is 40 times higher than that of the clinically approved PTX (TAXOL®) [13]. The POx-PTX formulation has favorable *in vivo* safety profile, higher maximum tolerated dose (MTD) and greater *in vivo* efficacy compared to PTX [14]. Notably, POx micelle platform is versatile and can deliver many APIs with different chemical structures and pharmacological activities [15].

Here we describe a multimodal theranostic nanoparticle platform, NanoFerrogels (NFGs), based on magnetite MNPs and POx block copolymers for drug delivery, noninvasive imaging and remote magneto-mechanical actuation of drug release. These novel materials contain two distinct structural domains - magnetite MNPs and POx-based polymeric micelles connected with each other and assembled in a stable nanoscale aggregate. The magnetite MNPs domains serve both as “beacons” for magnet and receptors for magneto-mechanical actuation, while the POx micelle domains serve for high-capacity loading of the drug (PTX).

2. Experimental Section

2.1. Materials

Benzyl alcohol and iron (III) acetylacetonate for MNPs synthesis, extra dry acetonitirle, methyl trifluoromethanesulfonate, valerontrile, ethanolamine, cadmium acetate dihydrate, 2-methyl-2-oxazoline, 1-Boc-piperazine for POx synthesis, nitric acid (TraceSELECT) and inductively coupled plasma mass spectrometry (ICP-MS) grade standards for iron (Fluka) for ICP-MS, 3,4-dihydroxyphenethylamine (dopamine), 3-[4,5-dimethylthiazol-2-yl]-2,5-diphenyl-tetrazolium bromide (MTT) were purchased from Sigma-Aldrich Inc. (St. Louis, MO, USA). PTX was purchased from LC Laboratories (Woburn, MA, USA). Dissuccinimidyl suberate (DSS), acetonitrile (ACN, HPLC grade), anhydrous methanol (MeOH), anhydrous n,n-dimethyl-formamide (DMF), dimethyl sulfoxide (DMSO), phosphate-buffered saline (PBS) and all other HPLC grade solvents were purchased from Fisher Scientific Inc. (Fairlawn, NJ, USA). Lysotracker® Red-DND 99, Hoechst 33342, Oregon Green® 488-conjugated PTX (OG488-PTX), and Alexa Fluor®-647-N-hydroxysuccinimide (AF647-NHS) were purchased from Thermofisher Scientific (Waltham,

MA, USA). All cell culture-related materials were purchased from Gibco (Gaithersburg, MD, USA).

Breast cancer cell lines, MCF-7, MDA-MB-231 and BT474 were supplied from American Type Culture Collection (ATCC, Manassas, VA, USA). MDA435/LCC6 (LCC-6-WT), MDA/LCC6^{mdr1} (LCC-6-MDR) cells were kindly donated by Dr. R. Clarke, Georgetown University Medical school [16]. The origin of the parent of these cells was questioned in literature [17], but they are commonly characterized as breast cancer [18]. All cells except BT474 were cultured in Dulbecco's modified eagle medium (DMEM) with 10 % fetal bovine serum (FBS) and 1 % Penicillin/streptomycin at 37 °C in a 5 % CO_2. BT474 cells were cultured in Roswell Park Memorial Institute medium (RPMI) 1640 with 2 mM L-glutamine, 1.5 g L^{-1} sodium bicarbonate, 4.5 g L^{-1} glucose, 10 mM (HEPES), 1.0 mM sodium pyruvate, and 0.01 mg mL^{-1} insulin with 10 % FBS and 1 % Penicillin/streptomycin at 37°C in a 5 % CO_2 incubator.

2.2. Methods

2.2.1. Synthesis of PTX-NFGs—The amphiphilic triblock copolymer P[$MeOx_{37}$-b-$BuOx_{20}$-b-$MeOx_{41}$] (P2) was synthesized by living cationic ring opening polymerization as described previously [13]. All substances, such as monomers 2-methyl-2-oxazoline (MeOx), 2-n-butyl-2-oxazoline (BuOx)), initiators, were dried by reflux with calcium hydride CaH_2, and distilled under inert argon immediately before the polymerization. The molecular weight and block length of the P2 were confirmed by ^{1}H NMR spectroscopy (M_n = 9.3 kg/mol, $PMeOx_{37}$-b-$PBuOx_{20}$-b-$PMeOx_{41}$), and GPC (Mn = 7.8 kg/mol, PDI = 1.18). The procedure of dopamine terminal conjugation to P2 was modified from Tong et al [19]. Briefly, piperazine-terminated P2 (100 mg) was dissolved in anhydrous MeOH and mixed with excess amount of (10-fold molar excess) of DSS in anhydrous DMF (1 mL). Sodium borate buffer (0.1 M, pH 8.0) was added to the solution, and it was incubated for 1 hr at room temperature (RT) under constant magnetic stirring at 400 rpm. Unreacted DSS was removed by gel filtration (Sephadex LH-20) with anhydrous MeOH as eluent. Activated POx-DSS was collected, and the solvent was evaporated *in vacuo*. Twenty-fold molar excess of dopamine was dissolved in anhydrous MeOH (2 mL) and added to activated P2-DSS (in 2 mL anhydrous MeOH). The solution was stirred overnight at 4°C. Excess of dopamine and other impurities were removed by dialysis (MWCO 3.5 kDa).

MNPs were synthesized by thermal decomposition of iron (III) Acetylacetonate ($Fe(acac)_3$) in anhydrous benzyl alcohol as described by Pinna et al [20], with minor modifications [21]. Briefly, 6.2 μmols of $Fe(acac)_3$ was mixed in three-necked flask with 45 mL of anhydrous benzyl alcohol. The reaction mixture was heated up to 110°C and incubated for 1 hr to remove moisture. Once the moisture was completely removed, temperature was gradually increased to 205°C at a rate of approximately 2°C min^{-1}, and the mixture was incubated at 205°C for 40 hr. The formed MNPs were precipitated and washed by acetone under magnet decantation, and residual organic solvent was completely evaporated by rotary evaporator. The MNPs were characterized by transmission electron microscopy (TEM), and superconducting quantum interference device (SQUID) to determine their size distribution, and saturation magnetization, respectively. Iron content in the PTX-NFGs was analyzed by

Inductively Coupled Plasma Mass Spectroscopy (ICP-MS; NexION 300D, Perkin Elmer, Waltham, MA). Briefly, 1 mg/mL of PTX-NFG solution was digested in 70% nitric acid, and incubated at 70°C for at least 12 hr. Following digestion, sample solution was further diluted in deionized (DI) water. Final concentration of nitric acid was adjusted to 2% and the samples were analyzed by ICP-MS.

PTX-loaded polymeric micelles were prepared by film hydration method [13]. Briefly, pre-determined amount of polymer (POx and/or POx-Dopamine) and PTX were dissolved in ethanol, the organic solvent was evaporated by airflow under mild heating (45°C). To remove residual ethanol, sample was kept *in vacuo* overnight. To form the micelles, DI water was added, and the mixture was incubated at 60°C for 20 min. Once formed, the micelle solution was cooled down to RT, and centrifuged at 10,000 rpm for 3 min to remove unloaded PTX. MNPs (0.5 mg mL^{-1}) were dispersed in DI water, sonicated using probe sonicator (500 V, 2 kHz, 20 % power, 10 seconds on, 5 seconds off) for 30 min, and added dropwise to dopamine-modified polymeric micelles. The mixture was stirred at 400 rpm for 24 hr. PTX-NFGs were purified by gel filtration (Sephadex G-25, DI water as eluent), and samples were lyophilized till future use.

2.2.2. PTX analysis—The PTX content in the formulations was quantified by high performance liquid chromatography (HPLC, Agilent Technologies 1200 Series, 250mm × 4.6 mm Phenomex C18- 5 μm column). The mobile phase was ACN:H_2O (55:45 v/v), flow rate was 1.0 mL min^{-1}, column temperature was 40°C. and the detection wavelength was 227 nm. Retention time for PTX was 6 min. To extract the PTX, the samples (70 μL) were mixed with acetonitrile (140 μL), sonicated and incubated for 30 min. The NFGs were separated by centrifugation at 12,000 rpm for 60 min, and supernatant was collected under magnet decantation. Twenty microliters of the supernatant were injected into HPLC.

2.2.3. Size and zeta potential measurements—The particle size of PTX-NFGs, was determined by nanoparticle tracking analysis (NTA) (Nanosight NS500, Wiltshire, United Kingdom, NTA 2.0 analytical software). Samples were prepared at concentration of 50 μg mL^{-1} with approximate particle concentration of 10^8 particles mL^{-1}. A 60 sec video was recorded and analyzed by NTA software. Zeta-potential of formulation was measured using a Malvern Zetasizer (Malvern Instruments, Malvern, UK). The samples were diluted to 1.0 mg mL^{-1} in DI water, and inserted disposable zeta cells were used for the measurements. Particle size of dopamine conjugated POx micelles (1 mg mL^{-1}) was determined by dynamic light scattering (Malvern Instrument, Malvern, UK).

2.2.4. Transmission electron microscopy (TEM)—TEM images of the uncoated MNPs, and PTX-NFGs were taken by JEOL 2010F-FasTEM (Peabody, MA, USA). The samples were diluted to approximately 0.25 mg mL^{-1} in DI water. A drop of diluted sample was put onto a carbon-coated copper grid (TedPella Inc., Redding, CA, USA) and dried in air. A drop of 5 % uranyl acetate was added on the TEM grid for negative staining. The particle size and size distribution of uncoated MNPs were calculated by ImageJ software (NIH, Bethesda, MD, USA).

2.2.5. Saturation magnetization measurements—The saturation magnetization was measured using superconducting quantum interference device-vibrating sample magnetometer (SQUID-VSM; Quantum Design Co.). Pre-weighted samples were placed in sample holder and mounted in a transparent straw and the magnetization was determined at 300°K.

2.2.6. *In vitro* PTX release—The *in vitro* release rate of PTX from the formulation was evaluated by the membrane dialysis method [22]. Each formulation was diluted with 40 g L^{-1} bovine serum albumin (BSA) solution in PBS to a final sample concentration of 50 μg mL^{-1} PTX. 100 μL of diluted samples were placed in dialysis tubes (Slide-A-Lyzer, 20 kDa MWCO, Thermo Scientific, Rockford, IL, USA) and dialyzed against 20 mL of 40 g L^{-1} BSA solution in PBS. All samples were kept at 37°C and shaken. At predetermined time point, samples were removed, and PTX concentration in the dialysis tube was measured by HPLC as described in section 2.2.2.

2.2.7. Intracellular distributions of PTX-NFGs—The AF647-labelled POx was synthesized by reacting POx in anhydrous methanol (10 mg mL^{-1}) with AF647-NHS (5 molar excess) in DMSO. The mixture was stirred for 2 hr at RT. Free AF647, was removed by gel filtration (Sephadex LH-20, MeOH as eluent). Fluorescent labeled PTX-NFGs were prepared as described in section 2.2.1. The ratio of AF647-POx to POx was 1:20 and the ratio between OG488-PTX and PTX was 1:10. MCF-7 cells were seeded in 8 well Lab-Tek II chamber slides at 1×10^5 cells $well^{-1}$, and allowed to grow for 48 hr. Cells were treated with fluorescent labelled PTX-NFG (200 μg mL^{-1}) for 4 or 24 hr. Following the treatment, the media containing PTX-NFG were removed, and the cells were washed 3 times with PBS. Next, the cells were treated with 100 nM of Lysotracker® Red DND-99 for 1hr, washed with PBS, treated with Hoechst 33342 nuclei staining for 15 min and washed with PBS. The cells were fixed with 4 % paraformaldehyde (PFA) for 15 min and washed with DI water. Intracellular distribution was assessed by confocal microscopy using Carl Zeiss 700 confocal laser scanning microscope with 40x/1.4 oil plan apo lens and the degree of colocalization was quantified by coloc2 plugin from ImageJ software [23,24].

2.2.8. Cytotoxicity of PTX-NFGs—*In vitro* cytotoxicity of PTX-NFGs was assessed by MTT assay [25]. Cells were seeded at 5,000 cells $well^{-1}$ in a 96-wells plate, and allowed to grow for 24 hr. Cells were incubated with the PTX-NFGs for 24 hr. After treatment, medium was removed, and cells were incubated with fresh medium for 72 hr. MTT reagent (1 mg mL^{-1}) was added and the cells were incubated for 4 hr. The medium was removed, the formazan salt was solubilized in DMSO, and the absorbance was read at 562 nm using a plate reader (SpectraMax M5, Molecular Devices Co., USA). Cell survival % was calculated as A_{treat} given by $A_{control} \times 100$. IC_{50} was determined using GraphPad Prism software (GraphPad Software INC., San Diego, CA, USA).

2.2.9. *In vitro* Relaxivity Measurements—The transverse relaxivities of the PTX-NFGs were measured on the 3T Siemens Magnetom Prisma (Siemens Medical Solutions, Malvern, PA, USA). PTX-NFGs were dissolved in DI water, and serially diluted (0, 0.018, 045, 0.09, 0.18, 0.27 and 0.36 mM Fe). The sequence for T_2 mapping was modified

from Vishwasaro et al [21]. Briefly, Carr-Purcell-Meiboom-Gill phase cycled single slice multi-echo sequence was used. Thickness of coronal image was 2 mm with 320 × 320 mm^2 acquisition matrix, and 220 mm field of view. Total 32 echos from 10 ms to 320 ms were collected (10 ms echo spacing). Relaxation time (T_2) was measured and converted to relaxation rates ($R_2 = 1 \times T_2^{-1}$). Transverse molar relaxivity values (r_2) were calculated as the slope of the plots of the R_2 as function of Fe concentration.

2.2.10. *In vivo* MRI imaging—Animal use followed the policies of the University of North Carolina at Chapel Hill Institutional Animal Use and Care Committee. All animals acclimated in the animal facilities before experiments. Animals were exposed to a 12 hr light/dark cycle and received food and water ad libitum throughout the studies. Female athymic nude mice (6–8 weeks of age) were inoculated with 5×10^6 human LCC-6-WT cancer cells, resuspended in 50 % growth medium and 50 % Matrigel (BD Biosciences) by orthotopic implantation. When tumor volume reached *ca.* 500 mm^3, 6 animals were randomized into 2 groups of mice (n=3) with similar mean tumor volumes in each group and then treated with following formulations: (1) NFG/E (23 mg kg^{-1} Fe), and (2) FERAHEME® (Ferumoxytol injection 23 mg kg^{-1} Fe). The formulations were administered i.v *via* tail vein. Saline was chosen as a frame reference. T2-weighted imaging was performed on a 9.4-T scanner (Bruker Scientific Instruments, Billerica, MA) with 35 mm quad-transceiver volume coil using a Turbo-RARE sequence (TR/TE, 3858.12 ms/ 10.85 ms; slice thickness, 0.5 mm). Images were acquired before and 1, 5, and 24 hours after intravenous (IV) administration. To calculate Signal intensity (SI) operator-dependent regions of interest (ROIs) were used in the T2-weighted, TE (10.85 ms) images of tumor and lymph nodes obtained before and 24 post MNP injection. Saline was chosen as a frame of reference.

2.2.11. Remote actuation by super-low frequency magnetic field—For these studies we used a custom designed super low frequency alternating current (AC) magnetic field generator with variable power (up to 1.5 kW), frequency (30 to 3000 Hz) and magnetic field amplitude (10 to 100 mT) (Nanomaterials Ltd; Tambow, Russia). The temperature controlled holder accommodates either drug release dialysis device or strip plate for cytotoxicity studies. The temperature was maintained at 37 °C for all experiments.

For the PTX release studies PTX-NFG/B formulation was diluted with 40 g L^{-1} BSA in PBS to a final concentration of 0.5 mg mL^{-1}. One hundred μL of sample was placed in dialysis tube and exposed to AC magnetic field (50 kA m^{-1}, 50 Hz) for 30 min continuously. After exposure to AC magnetic field, dialysis tubes were placed in 20 mL 40 g L^{-1} BSA in PBS at 37°C under shaking (50 rpm). Non-treated samples were directly immersed in 20 mL release media at 37°C under shaker (50 rpm). At predetermined time point, samples were removed, and PTX concentration in the dialysis tube was measured by HPLC as described in section 2.2.2.

Cell viability: LCC-6-WT cells were seeded at 5,000 cells per well in 2×8 MICROLON 96 well high binding plate strips (Greiner Bio INC., USA) and were allowed to adhere for 72 hrs. Cells were treated with NFG-E at various concentration (MNP concentration range 10–150 μg mL^{-1}) for 24 hrs at 37 °C, washed with acidic saline (pH 3.0), filled with fresh

media, and exposed to 50 Hz AC magnetic fields of 50 kA m^{-1} for 30 min. In the pulsed exposure mode, the cells were exposed to the field with a 10 min on, 5 min off pattern for total on field exposure of 30 min. Cell viability was measured 4 hr after exposure using CCK study (Dojindo, Japan).

2.2.12. Statistical Analyses—All statistical analyses was performed using Graphpad Prism. All data represented as mean ± S.D. Comparison between two groups was done by two-tailed Student's t-test, and comparison between more than two groups were assessed by one-way ANOVA with Dunnect's post-hoc test. For *in vivo* MRI imaging study, comparison between more than three groups were assessed by two-way ANOVA with Ryan-Einot-Gabriel-Welsc's post-hoc test (*p<0.05, **p<0.01, ***p<0.001).

3. Results

3.1. Synthesis of PTX-NFGs

The size and size distribution of MNPs can be fine-tuned during the MNPs synthesis by optimizing the heating schedule [21]. In this study, we produced uniform superparamagnetic MNPs with 5.5±1.1 nm diameter and saturation magnetization of 80 emu g^{-1} (supplementary Fig. S1A–C) and used them in all experiments described here. The NFGs were manufactured by reacting the MNPs with PTX loaded dopamine decorated POx micelles in aqueous media. Dopamine, a member of the catecholamine family, has high binding affinity to iron oxide and was conjugated to piperazine-terminated POx copolymer P[$MeOx_{37}$-b-$BuOx_{20}$-b-$MeOx_{41}$] (P2) to anchor the micelles to the surface the MNPs [26]. Dopamine was conjugated to POx using DSS, selective non-cleavable amine to amine linker (supplementary Fig. S2A). ^{1}H-NMR showed that ~100 % of polymer chains were successfully modified with dopamine (supplementary Fig. S2B,C). Notably, dopamine conjugation did not affect the ability of POx to form micelles and load PTX. No significant differences in particle size, PDI, and loading capacity of PTX were observed compared to dopamine free POx-PTX micelles (supplementary Fig. S3).

To prepare the PTX-NFGs while avoiding hydrolysis of PTX ester groups in alkaline pH [27] and the oxidation of dopamine to dopaquinone [28,29] we slightly modified the procedure of PTX-NFGs synthesis. The MNPs were dispersed in DI water at neutral pH (pH~7.0), sonicated for 30 min (to minimize the aggregation of MNPs) and mixed with the pre-prepared PTX-POx micelles (Fig. 1A). The PTX to POx feeding ratio in these micelles was 2:10 w/w. We prepared six formulations of PTX-NFGs by mixing MNP with either 20% or 100% PTX-POx-Dopamine (Fig. 1B, Table 1). To confirm that PTX content in the NFGs could be increased without loss of stability, we also prepared PTX-NFGs at 1:1 w/w loading ratio (supplementary Table S1).

Formation of PTX-NFGs did not affect the PTX loading (LE of PTX remained around 100 %). MNPs were effectively loaded into PTX-NFGs, LE of MNPs was in 60–70 % range. The LC of MNPs in PTX-NFGs varied between 0.3–11.9 % w/w. As expected, the NFGs prepared with the 100 % POx-Dopamine had the highest MNPs loading, reaching 11.9 % w/w for PTX-NFG/D, synthesized at 1:4 ratio of MNPs to POx-Dopamine.

3.2. Physicochemical characterization of PTX-NFGs

All PTX-NFGs samples had an average hydrodynamic diameter from 100 nm to 130 nm as determined by NTA (Fig 2A, supplementary Fig. S4). The PTX-NFGs prepared with 20% POx-Dopamine had a high positive ξ-potential of +25–30 mV, like that of POx-micelles, which was obviously due to the presence of the protonated amino groups in the terminal piperazine moieties of POx. The PTX-NFGs prepared with 100% POx-Dopamine showed ξ-potential of up to 10 mV, comparable to ξ-potential of POx-Dopamine micelles (Fig. 2B). The morphology of PTX-NFGs examined by TEM (Fig. 2D), revealed raspberry-like clusters with multiple electron dense grains of MNPs that appeared to be surrounded by polymeric species, possibly free POx micelles. The average size of the clusters as measured by TEM was around 100 nm, i.e., comparable to the NTA size data. PTX-NFGs displayed superparamagnetic behavior without any significant remnant magnetization (Fig. 2C). The saturation magnetization of PTX-NFGs gradually decreased as the POx-dopamine content in PTX-NFGs increased (Table 2), which is likely due to interactions between the polymer and MNPs [30,31].

3.3. Colloidal stability of PTX-NFGs

The colloidal stability of PTX-NFGs was determined by measuring the particle size by NTA as well as visual assessment of phase separation over time (Fig. 3, supplementary Fig. S5). While the particle size did not seem to change dramatically during the time of the observation (days), the formation of precipitate observed in various samples was indicative of the loss of stability. The POx-Dopamine content in the formulation had major influence on the stability of PTX-NFGs. Specifically, all formulations with 20% POx-Dopamine were stable in dispersion with no sign of phase separation for at least 1 day and exhibited precipitation on day 2 or day 3. In contrast, all formulations with 100% POx-Dopamine content precipitated during day 1. Similar trend was observed for the formulations dispersed in PBS (Fig. 3) as well as DI water (supplementary Fig. S5), although the particle size changes over time were more pronounced in DI water than those in PBS. This suggests that the precipitation was not due to the phosphate anions-induced desorption of the polymer discussed previously [21], but rather restructuring and aggregation of the PTX-NFGs particles.

3.4. *In vitro* release of PTX

PTX release studies were performed in BSA solution in PBS (40 g L^{-1}) to establish sink conditions for PTX [32]. PTX has a high binding affinity to serum albumin [33,34] and mostly circulates in albumin bound form post IV administration [14]. All PTX-NFGs showed sustained release profile with no burst release (Fig. 4). The release of PTX from 100 % POx-Dopamine decorated NFGs (PTX-NFGs/D-F) was similar to PTX release from PTX/POx micelles (Fig. 4A). However, the PTX release from 20 % POx-Dopamine decorated NFGs (PTX-NFGs/A-C) was slower compared to PTX/POx micelles. Specifically, during first 8 h PTX/POx micelles released over 40% of PTX compared to approximately 20 % released from PTX-NFGs/A-C formulations (Fig. 4B). (The compassion of the release profiles from the 20% and 100% POx-Dopamine decorated NFGs is further detailed in the

supplementary Fig. S6). Notably, alteration in the MNPs content in these compositions had little if any effect on the PTX release profiles.

3.5. Intracellular distribution of PTX-NFGs

To validate the safety of our formulations we determined the cytotoxicity of blank NFGs in MCF-7 and LCC-6-MDR breast cancer cells (supplementary Fig. S7). The NFGs were nontoxic in both cell lines in the entire range of MNPs concentrations tested. For the intracellular uptake and distribution studies we used PTX-NFG/B, the formulation with the highest colloidal stability. The intracellular uptake and distribution of PTX-NFG/B in MCF-7 cells was studied by confocal microscopy (Fig. 5A). To track the drug and polymer distribution in the cells the fluorescently labeled PTX (OG488-PTX) and POx (AF647-POx) were used. Both POx and PTX were rapidly internalized and colocalized ith the lysosomes (yellow punctate regions) as early as at 4 h of exposure. At that time point over 75 % of AF647-POx and OG488-PTX were colocalized with the lysosomes (Fig. 5B). At the longer incubation time of 24 h there was a slight but significant decrease in the colocalization between PTX and lysosomes compared to 4 h time point (4h: 76.6±4.5 %; 24h: 62.9±8.3%, $p<0.001$) with ~63 % and ~37% of the drug found in the lysosomes and cytoplasm respectively (Fig. 5B).

3.6. *In vitro* cytotoxicity of PTX-NFGs

The *in vitro* cytotoxicity of the PTX-NFGs was determined in 3 breast cancer cell lines: human breast adenocarcinoma MCF-7, triple negative human breast adenocarcinoma LCC-6-WT, and triple negative multidrug resistant human breast adenocarcinoma LCC-6-MDR (Table 3 and supplementary Fig. S8). All PTX-NFGs exhibited similar cytotoxicity compared to free PTX in MCF-7, and LCC-6-WT. Some of the PTX-NFGs formulations (PTX-NFG/A, PTX-NFG/D and PTX-NFG/E) had lower IC_{50} values compared to free PTX in LCC-6-MDR cells, however, the differences were several folds only. Separately, we characterized the cytotoxicity of the empty NFGs in each of the cell lines listed in Table 3. Of the three cell lines the empty NFGs were more cytotoxic in LCC-6-WT cells (as discussed below). However, even in this case no-cytotoxic effect was observed until 10 μg/ml NFGs concentration. The thresholds for the cytoxicity of NFGs was even higher for the two other cell lines: ~100 μg/ml for MCF-7 and ~150 μg/ml for LCC-6-MDR cells. All these values were at least two orders of magnitude higher than the concentration of the NFGs in the cytotoxicity studies (at IC_{50} of the drug) and therefore the observed IC_{50} values and cytotoxicity of PTX-NFGs are due to the cytotoxic effects of the drugs incorporated in these nanoformulations.

3.7. Enhanced drug release from PTX-NFGs induced by AC magnetic field

In order to evaluate the effect of the super-low frequency AC magnetic field on PTX release, PTX-NFG/B was dissolved in 40 g L^{-1} of BSA/PBS media, and exposed to AC magnetic field (50 Hz, 50 kA m^{-1}, 30 min) starting at 1 h of incubation (Fig. 6A). One set of samples was exposed three times of AC magnetic field (1h, 2h, 3h) and the PTX release was measured at 4 h time point. The second set of samples was exposed to five times, (1h, 2 h, 3 h, 4 h and 6 h) and the PTX release was measured at 8 h time point. At both 4 and 8 h time points, PTX release in the samples exposed to the magnetic field was significantly higher

compared to non-exposed samples, 29.3 % vs. 13.3% at 4h and 47.6 % vs. 19.7 at 8 h (Fig. 6B).

3.8. Cytotoxic effect of NFGs in cancer cells induced by AC magnetic field

To evaluate the effects of the AC magnetic field on the cells viability, we incubated LCC-C6-WT breast cancer cells with NFG/E at concentrations up to 150 μg ml^{-1} MNPs equivalent (Fig. 6C, D). Following incubation with various concentration of NFGs for 24 hr, the cells were exposed to continuous (50 kA m^{-1}, 50 Hz, 30 min) or pulsed (10 min "on" / 5 min "off", total "on" 30 min) AC magnetic field or no field treatment as previously described [35]. Although exposure to higher concentrations of MNPs (above 10 μg mL^{-1}) induced some cytotoxicity even without the field, pulsed AC magnetic field indeed reduced the cell viability by about 40 % at the concentration of MNPs as low as 10 μg mL^{-1}. As the uptake and colocalization studies showed that the NFGs accumulate mainly in lysosomes (Fig. 5B), the mechanism of cells disruption is likely to be similar to the previously reported cytoskeleton disruption pathway [35].

3.9. *In vitro* relaxivity measurements

To measure the T2 relaxivity *in vitro* we prepared a series of PTX-NFGs solutions in DI water and imaged them on 3T MRI (supplementary Fig. S9A). The relaxivity rate (R_2) at 3T was plotted as function of Fe concentration (supplementary Fig. S9B). The slope of the plot, the r_2 value, was calculated and compared for different PTX-NFGs formulations (Table 4). The relaxivity values were in the range of 13.8–30.3 $s^{-1}mM^{-1}$ that is lower than the r_2 values of commercial agents Feridex® and Ferumoxytol (r_2 = 148 $mM^{-1}s^{-1}$, and 62.3 $mM^{-1}s^{-1}$, respectively). Interestingly, the r_2 values were higher for the 20% dopamine modified NFGs (PTX-NFGs/A-C) despite low MNP content in these NFGs (PTX-NFG/A-C versus PTX-NFG/D-F).

3.10. *In vivo* MRI imaging

To evaluate the MRI contrast potential of drug-free NFGs, the mice bearing LCC-6-WT tumors were injected IV with NFG/E or Ferumoxytol. NGF/E was selected due to its stability and relatively high NMP loading. The injected dose (30 mg Fe kg^{-1}, equivalent to 2.4 mg Fe kg^{-1} in humans based on FDA conversion guidelines) was below the clinically used dose of 4 mg Fe kg^{-1} [36,37]. The T2 images were taken 1 h, 5 h and 24 h post injection (Fig. 7A) and the SI was calculated compared to the reference solution (supplementary Fig. S10A–C). At these respective time points the decreases in SI in the tumor following administration of NFG/E were 0.8%, 2.7%, and 2.7% compared to 10.5%, 11.7%, and 0% following Ferumoxytol administration (Fig. 7B). In the lymph nodes the SI decreased 24.9%, 26.6%, and 26.6% for NFG/E compared to 31.6%, 39.6%, and 18.1% for Ferumoxytol (Fig. 7C). Notably, even though Ferumoxytol had significantly higher r_2 compared to NFG/E *in vitro*, the SI decrease in the tumor 24 h after injection of Ferumoxytol was negligible, compared to detectable 2.7% for NFG/E (Fig. 7B). This effect was even more pronounced in the lymph nodes (18.1 versus 26.6) (Fig. 7C). Therefore, NFG/E displayed prolonged tumor and lymph nodes retention compared to that of Ferumoxytol.

4. Discussion

This work develops a new class of hybrid theranostic materials, NFGs, based on cross-linked raspberry-like nanoclusters of MNPs and POx micelles that have multiple functionalities for drug delivery, MRI imaging and remote magneto-mechanical actuation. In this study we report on the (1) synthesis of NFGs and their loading with a hydrophobic API, PTX, (2) the *in vitro* drug release from the drug PTX-loaded NFGs, (3) the use of these materials for MRI of tumors and lymph nodes *in vivo*, and (4) drug release and cancer cell death enhancement with these materials as a result of their remote actuation by super-low frequency AC magnetic field.

In order to load MNPs and PTX into two segregated compartments, we designed the system where MNPs were conjugated to drug-loaded pre-formed POx micelles. Therefore, PTX was in the hydrophobic core of the micelles, and the MNPs were bound to the dopamine-decorated micelle shell. This approach, of combining two segregated compartments, allowed to maintain the ultra-high drug loading capacity of P[$MeOx_{37}$-b-$BuOx_{20}$-b-$MeOx_{41}$] micelles for PTX [13]. Several studies described PTX-loaded MNPs formulations. However, the feeding ratio between polymer and PTX was 10:1 or higher (polymer: PTX) resulting in drug loading below 10 wt. % [38–42]. In this study we were able to achieve 20 % w/w to 50 % w/w drug loading.

Two methods are commonly used for MNPs synthesis, co-precipitation of ferrous and ferric ions with the presence of base (alkali aqueous solution) [43], and thermal decomposition of iron precursor. Although the MNPs formed by co-precipitation method have hydrophilic surface and can be dispersed in aqueous media, it is difficult to control their size, and size distribution. Thermal decomposition of organic iron precursor in non-aqueous solvent, such as benzyl ether, or benzyl alcohol allows better control of particle size [20,44]. Several groups screened functional moieties with high affinity to MNPs surface, such as carboxylates, phosphates and catechols. Specifically, dopamine (4-(2-Aminoethyl) benzene-1,2-diol), one of the analogs of catecholamine, can be used as an anchor group as it combines high affinity to MNPs surface with a free amine group for POx conjugation [28,29]. Although dopamine was covalently conjugated to POx block copolymer and no release of dopamine over time was observed, given the role of dopamine in central nervous system (CNS), it is critically important to assess the safety of dopamine-contained nanomaterials. Previously reported IC_{50} of dopamine *in vitro* in various cell line are in the range of 25 μM to 250 μM [45–47]. In our cytotoxicity experiments the highest POx-Dopamine concentration was 70 μg mL^{-1}, corresponding to dopamine concentration of less than 7.3 μM. The dopamine dosing in the *in vivo* imaging experiments was around 15.3 mg kg^{-1}. In both cases no toxicity was observed.

Previous studies have shown that colloidal stability of polymer coated MNPs, in which polymer was anchored to MNPs via dopamine anchor groups, depended on the [MNPs]: [dopamine] ratio [48,49]. For example, Lassenberger et al. developed nitrodopamine-PEG coated MNPs. Feeding ratio of [MNPs]/[nitrodopamine-PEG] was set at 10, and corresponding LC of MNPs was around 5 %. However, the particles were not stable in either DI water or PBS for more than 2 days [48]. We set the minimum [MNPs]/[POx-

Dopamine] ratio > 1 to increase the incorporation of MNPs into NFGs. Consistent with the previously reported data, PTX-NFGs prepared 20 % content of POx-Dopamine in the total POx polymer were more stable compared to NFGs prepared at 100 % POx-Dopamine. Also, the POx-Dopamine:POx ratio, but not the MNP:POx ratio affected the PTX release rates. Kim et al [12] reported that the release of drug from shell-crosslinked micelles was slower compared to non-crosslinked micelles as crosslinked shell represented a tight network, reducing the mobility of drug in the micelles core. Similar effect of crosslinking was observed by Teng and co-workers [50]. This is in agreement with our observation of slower PTX release from PTX-NFGs with 20 % dopamine, which contain POx micelles with the shells crosslinked through MNPs-dopamine interactions.

There are several factors that affect T_2 relaxivity of MNPs, such as size of MNPs [51–52], MNPs surface properties [51], degree of aggregation [52,53], coating hydrophilicity [54], surface modification [55] and thickness [5]. Coating of the MNPs strongly affects the T_2 relaxivity as coating can either reduce or increase water molecules penetration to MNPs therefore reducing or enhancing relaxivity. Compared to other functional MNP formulations, the relaxivity of our NFG was relatively low. Tong et al. [56]. measured T_2 relaxivity of MNPs coated with PEG with five different PEG chain lengths (550 to 5,000 Da). The T_2 relaxivity of MNPs coated with PEG5000 was almost 8 times lower compared to MNPs coated with PEG 550 due to lower permeability of water through the polymer coating [56].

Interestingly, at same MNP : POx-Dopamine ratio the transverse relaxivity r_2 was higher for PTX-NFG/A-C compared to PTX-NFG/D-F that differ in the percent of POx-Dopamine. The explanation could be complex, but we would like to point out the difference in the charges between these two groups of NFGs. It was previously reported that MRI relaxivity can be affected by nanoparticle surface charge [57]. MNPs bearing positive charge displayed higher r_2 than neutral or negatively charged MNPs. Additionally, the presence of hydrophilic polymer coating around MNPs can slow down water diffusion and contribute to R_2 increase [58,59]. Therefore, greater transverse relaxivity observed for PTX-NFG/A-C group is consistent with positive zeta-potential and high content of unconjugated POx in these systems compared to PTX-NFG/D-F group.

Although *in vitro* T_2 relaxivity values are important for prediction of *in vivo* performance, biodistribution and tissue incorporation of nanoparticles also play a major role. T_2-enhancement in relatively early post-contrast scans is affected by the tumor's blood volume, which contributes as much as 5 % to SI for most cancers [60,61]. Therefore, SI at later time points is usually due to uptake and retention of contrast agents in tumor and tumor associated macrophages [62]. It is likely, therefore, that 24 h post injection, Ferumoxytol is cleared from the tumor site and lymph nodes, while NGFs are retained and provide significant uniform contrast reduction.

Previous studies showed that magneto-mechanical actuation of MNPs under super-low frequency magnetic field induced conformational and functional changes of the surrounding materials. Klyachko et al. [63] suggested that the rotation of MNPs in the AC magnetic field (50 Hz) generates shear and tensile stress forces, that induce structural deformation and deactivation of enzymes immobilized on MNPs. Zhang et al developed MNP conjugated

with LAMP1 antibody (lysosomal-associated membrane protein), which could be used to remotely activate apoptosis by rupturing the lysosomal membrane [64]. Previously Master et al. reported that the exposure of cells loaded with MNPs to the super-low frequency magnetic field led to the cytoskeleton disruption and subsequent cell death without any rupture of the lysosomal membrane [35]. Notably, the exposure to the pulsed AC magnetic field generated more cell damage than the continuous field. It was suggested that during the field exposure lysosomes with MNPs form needle-like structure and following exposure these structures disassemble. In the pulsed field regime, the repeated assembly/disassembly of lysosomes produce repeated stress-relaxation that may cause more damage to the cytoskeleton than the continuous field. Likewise, the pulsed magnetic field produced greater conformation changes and inactivation of enzymes immobilized on MNPs [63].

The observation of enhanced drug release from polymeric micelles by super-low frequency magnetic field is new to the best of our knowledge. The majority of previous studies in this area focused on temperature-induced changes in heat sensitive polymers and lipids during exposure to high frequency magnetic field (magnetic hyperthermia) [6,7]. Although the effect of the field exposure on drug release was dependent on the NFGs structure, the NFGs show the potential to combine both triggered release and MNPs induced cell death.

5. Conclusions

In this study, a multifunctional “three-in-one” PTX-NFGs composed of dopamine-conjugated POx micelles cross-linked through MNPs was designed, and six different formulations were developed. The context of the dopamine-conjugated POx polymer in the overall polymer composition affected the particle stability and drug release profile of PTX-NFGs. PTX-NFGs showed similar cytotoxicity against various breast cancer cell lines compared to pure PTX *in vitro*. We demonstrate that NFGs have potential as MRI contrast agents *in vivo* since NFGs produced more durable SI in both tumor and lymph nodes compared to Ferumoxytol, a commercially available MRI contrast agent. NFGs induced cell death following exposure to super-low frequency AC magnetic field against several breast cancer cell lines. Exposure to super-low frequency AC magnetic field also triggered release of PTX from PTX-NFG *in vitro*. Taken together, these results highlight a potential of PTX-NFGs as a theranostic platform for cancer diagnosis and treatment.

Supplementary Material

Refer to Web version on PubMed Central for supplementary material.

Acknowledgement

This work was supported by the seed program pre-doctoral fellowship from the Triangle Materials Research Science and Engineering Center (t-MRSEC), the National Institutes of Health grant (1R21CA220148) and the Eshelman Institute for Innovation at the UNC Eshelman School of Pharmacy (RX03612424). We also acknowledge the technical support from Dr. Amar Kumbar from Chapel Hill Analytical and Nanofabrication Laboratory (CHANL) for TEM micrograph, Dr. Lew Reynolds from Department of Materials Science and Engineering, North Carolina State University for SQUID, Dr. Hong Yuan from the Center for Animal MRI and Biomedical Research Imaging Center at the University of North Carolina-Chapel Hill (UNC), and UNC Lineberger Comprehensive Cancer Research Center Biostatistics Core for assistance of statistical analysis.

REFERENCES:

1. Cherry SR Multimodality in vivo imaging systems: twice the power or double the trouble? Annu Rev Biomed Eng 2006, 8, 35–62, doi:10.1146/annurev.bioeng.8.061505.095728. [PubMed: 16834551]
2. Rudin M; Weissleder R Molecular imaging in drug discovery and development. Nature reviews Drug discovery 2003, 2, 123. [PubMed: 12563303]
3. McCarthy JR; Weissleder R Multifunctional magnetic nanoparticles for targeted imaging and therapy. Adv Drug Deliv Rev 2008, 60, 1241–1251, doi:10.1016/j.addr.2008.03.014. [PubMed: 18508157]
4. Parvanian S; Mostafavi SM; Aghashiri M Multifunctional nanoparticle developments in cancer diagnosis and treatment. Sensing and Bio-Sensing Research 2017, 13, 81–87, doi:10.1016/j.sbsr.2016.08.002.
5. Bao G; Mitragotri S; Tong S Multifunctional nanoparticles for drug delivery and molecular imaging. Annu Rev Biomed Eng 2013, 15, 253–282, doi:10.1146/annurev-bioeng-071812-152409. [PubMed: 23642243]
6. Ito A; Shinkai M; Honda H; Kobayashi T Medical application of functionalized magnetic nanoparticles. J Biosci Bioeng 2005, 100, 1–11, doi:10.1263/jbb.100.1. [PubMed: 16233845]
7. Lu AH; Salabas EL; Schüth F Magnetic nanoparticles: synthesis, protection, functionalization, and application. Angew Chem Int Ed Engl 2007, 46, 1222–1244, doi:10.1002/anie.200602866. [PubMed: 17278160]
8. Golovin YI; Gribanovsky SL; Golovin DY; Klyachko NL; Majouga AG; Master AM; Sokolsky M; Kabanov AV Towards nanomedicines of the future: Remote magneto-mechanical actuation of nanomedicines by alternating magnetic fields. Journal of Controlled Release 2015, 219, 43–60, doi:10.1016/j.jconrel.2015.09.038. [PubMed: 26407671]
9. Alexiou C; Arnold W; Klein RJ; Parak FG; Hulin P; Bergemann C; Erhardt W; Wagenpfeil S; Lubbe AS Locoregional cancer treatment with magnetic drug targeting. Cancer research 2000, 60, 6641–6648. [PubMed: 11118047]
10. Kohler N; Sun C; Fichtenholtz A; Gunn J; Fang C; Zhang M Methotrexate-immobilized poly(ethylene glycol) magnetic nanoparticles for MR imaging and drug delivery. Small 2006, 2, 785–792, doi:10.1002/smll.200600009. [PubMed: 17193123]
11. Arias JL; Ruiz M; Gallardo V; Delgado AV Tegafur loading and release properties of magnetite/poly(alkylcyanoacrylate) (core/shell) nanoparticles. Journal of controlled release : official journal of the Controlled Release Society 2008, 125, 50–58, doi:10.1016/j.jconrel.2007.09.008. [PubMed: 17949844]
12. Kim Y; Liemmawal ED; Pourgholami MH; Morris DL; Stenzel MH Comparison of Shell-Cross-Linked Micelles with Soft and Glassy Cores as a Drug Delivery Vehicle for Albendazole: Is There a Difference in Performance? Macromolecules 2012, 45, 5451–5462, doi:10.1021/ma300644v.
13. Luxenhofer R; Schulz A; Roques C; Li S; Bronich TK; Batrakova EV; Jordan R; Kabanov AV Doubly amphiphilic poly(2-oxazoline)s as high-capacity delivery systems for hydrophobic drugs. Biomaterials 2010, 31, 4972–4979, doi:10.1016/j.biomaterials.2010.02.057. [PubMed: 20346493]
14. He Z; Wan X; Schulz A; Bludau H; Dobrovolskaia MA; Stern ST; Montgomery SA; Yuan H; Li Z; Alakhova D; et al. A high capacity polymeric micelle of paclitaxel: Implication of high dose drug therapy to safety and in vivo anti-cancer activity. Biomaterials 2016, 101, 296–309, doi:10.1016/j.biomaterials.2016.06.002. [PubMed: 27315213]
15. Han Y; He Z; Schulz A; Bronich TK; Jordan R; Luxenhofer R; Kabanov AV Synergistic combinations of multiple chemotherapeutic agents in high capacity poly(2-oxazoline) micelles. Mol Pharm 2012, 9, 2302–2313, doi:10.1021/mp300159u. [PubMed: 22681126]
16. He Z; Schulz A; Wan X; Seitz J; Bludau H; Alakhova DY; Darr DB; Perou CM; Jordan R; Ojima I; et al. Poly(2-oxazoline) based micelles with high capacity for 3rd generation taxoids: preparation, in vitro and in vivo evaluation. J Control Release 2015, 208, 67–75, doi:10.1016/j.jconrel.2015.02.024. [PubMed: 25725361]

17. Rae JM; Creighton CJ; Meck JM; Haddad BR; Johnson MD MDA-MB-435 cells are derived from M14 melanoma cells--a loss for breast cancer, but a boon for melanoma research. Breast cancer research and treatment 2007, 104, 13–19, doi:10.1007/s10549-006-9392-8. [PubMed: 17004106]

18. Yuan K; Frolova N; Xie Y; Wang D; Cook L; Kwon Y-J; Steg AD; Serra R; Frost AR Primary cilia are decreased in breast cancer: analysis of a collection of human breast cancer cell lines and tissues. J Histochem Cytochem 2010, 58, 857–870, doi:10.1369/jhc.2010.955856. [PubMed: 20530462]

19. Tong J; Luxenhofer R; Yi X; Jordan R; Kabanov AV Protein modification with amphiphilic block copoly(2-oxazoline)s as a new platform for enhanced cellular delivery. Mol Pharm 2010, 7, 984–992, doi:10.1021/mp100102p. [PubMed: 20550191]

20. Pinna N; Grancharov S; Beato P; Bonville P; Antonietti M; Niederberger M Magnetite Nanocrystals: Nonaqueous Synthesis, Characterization, and Solubility. Chemistry of Materials 2005, 17, 3044–3049, doi:10.1021/cm050060+.

21. Vishwasrao HM; Master AM; Seo YG; Liu XM; Pothayee N; Zhou Z; Yuan D; Boska MD; Bronich TK; Davis RM; et al. Luteinizing Hormone Releasing Hormone-Targeted Cisplatin-Loaded Magnetite Nanoclusters for Simultaneous MR Imaging and Chemotherapy of Ovarian Cancer. Chemistry of Materials 2016, 28, 3024–3040, doi:10.1021/acs.chemmater.6b00197.

22. Han Y; He Z; Schulz A; Bronich TK; Jordan R; Luxenhofer R; Kabanov AV Synergistic combinations of multiple chemotherapeutic agents in high capacity poly(2-oxazoline) micelles. Molecular pharmaceutics 2012, 9, 2302–2313, doi:10.1021/mp300159u. [PubMed: 22681126]

23. Bolte S; Cordelières FP A guided tour into subcellular colocalization analysis in light microscopy. Journal of microscopy 2006, 224, 213–232, doi:10.1111/j.1365-2818.2006.01706.x. [PubMed: 17210054]

24. Schindelin J; Arganda-Carreras I; Frise E; Kaynig V; Longair M; Pietzsch T; Preibisch S; Rueden C; Saalfeld S; Schmid B; et al. Fiji: an open-source platform for biological-image analysis. Nature Methods 2012, 9, 676–682, doi:10.1038/nmeth.2019. [PubMed: 22743772]

25. van Meerloo J; Kaspers GJ; Cloos J Cell sensitivity assays: the MTT assay. Methods in molecular biology (Clifton, N.J.) 2011, 731, 237–245, doi:10.1007/978-1-61779-080-5_20.

26. Mazur M; Barras A; Kuncser V; Galatanu A; Zaitzev V; Turcheniuk KV; Woisel P; Lyskawa J; Laure W; Siriwardena A Iron oxide magnetic nanoparticles with versatile surface functions based on dopamine anchors. Nanoscale 2013, 5, 2692–2702. [PubMed: 23420060]

27. Tian J; Stella VJ Degradation of paclitaxel and related compounds in aqueous solutions II: Nonepimerization degradation under neutral to basic pH conditions. J Pharm Sci 2008, 97, 3100–3108, doi:10.1002/jps.21214. [PubMed: 17963215]

28. Lee H; Dellatore SM; Miller WM; Messersmith PB Mussel-Inspired Surface Chemistry for Multifunctional Coatings. Science 2007, 318, 426–430, doi:10.1126/science.1147241. [PubMed: 17947576]

29. Lee H; Scherer NF; Messersmith PB Single-molecule mechanics of mussel adhesion. Proc Natl Acad Sci U S A 2006, 103, 12999–13003, doi:10.1073/pnas.0605552103. [PubMed: 16920796]

30. Yuan Y; Rende D; Altan CL; Bucak S; Ozisik R; Borca-Tasciuc DA Effect of surface modification on magnetization of iron oxide nanoparticle colloids. Langmuir 2012, 28, 13051–13059, doi:10.1021/la3022479. [PubMed: 22889238]

31. Rahimi M; Yousef M; Cheng Y; Meletis EI; Eberhart RC; Nguyen K Formulation and characterization of a covalently coated magnetic nanogel. J Nanosci Nanotechnol 2009, 9, 4128–4134. [PubMed: 19916419]

32. Margarson MP; Soni N Serum albumin: touchstone or totem? Anaesthesia 1998, 53, 789–803. [PubMed: 9797524]

33. Cedervall T; Lynch I; Lindman S; Berggard T; Thulin E; Nilsson H; Dawson KA; Linse S Understanding the nanoparticle-protein corona using methods to quantify exchange rates and affinities of proteins for nanoparticles. Proc Natl Acad Sci U S A 2007, 104, 2050–2055, doi:10.1073/pnas.0608582104. [PubMed: 17267609]

34. Dutta D; Sundaram SK; Teeguarden JG; Riley BJ; Fifield LS; Jacobs JM; Addleman SR; Kaysen GA; Moudgil BM; Weber TJ Adsorbed proteins influence the biological activity and molecular

targeting of nanomaterials. Toxicological sciences : an official journal of the Society of Toxicology 2007, 100, 303–315, doi:10.1093/toxsci/kfm217. [PubMed: 17709331]

35. Master AM; Williams PN; Pothayee N; Pothayee N; Zhang R; Vishwasrao HM; Golovin YI; Riffle JS; Sokolsky M; Kabanov AV Remote Actuation of Magnetic Nanoparticles For Cancer Cell Selective Treatment Through Cytoskeletal Disruption. Scientific Reports 2016, 6, 33560, doi:10.1038/srep33560. [PubMed: 27644858]
36. (FDA), F.a.D.A. Food; Administration, D. Guidance for industry: estimating the maximum safe starting dose in initial clinical trials for therapeutics in adult healthy volunteers. Center for Drug Evaluation and Research (CDER) 2005, 7.
37. Toth GB; Varallyay CG; Horvath A; Bashir MR; Choyke PL; Daldrup-Link HE; Dosa E; Finn JP; Gahramanov S; Harisinghani M; et al. Current and potential imaging applications of ferumoxytol for magnetic resonance imaging. Kidney Int 2017, 92, 47–66, doi:10.1016/j.kint.2016.12.037. [PubMed: 28434822]
38. Cui Y; Xu Q; Chow PK; Wang D; Wang CH Transferrin-conjugated magnetic silica PLGA nanoparticles loaded with doxorubicin and paclitaxel for brain glioma treatment. Biomaterials 2013, 34, 8511–8520, doi:10.1016/j.biomaterials.2013.07.075. [PubMed: 23932498]
39. Dilnawaz F; Singh A; Mewar S; Sharma U; Jagannathan NR; Sahoo SK The transport of non-surfactant based paclitaxel loaded magnetic nanoparticles across the blood brain barrier in a rat model. Biomaterials 2012, 33, 2936–2951, doi:10.1016/j.biomaterials.2011.12.046. [PubMed: 22264522]
40. Jain TK; Richey J; Strand M; Leslie-Pelecky DL; Flask CA; Labhasetwar V Magnetic nanoparticles with dual functional properties: drug delivery and magnetic resonance imaging. Biomaterials 2008, 29, 4012–4021, doi:10.1016/j.biomaterials.2008.07.004. [PubMed: 18649936]
41. Schleich N; Po C; Jacobs D; Ucakar B; Gallez B; Danhier F; Preat V Comparison of active, passive and magnetic targeting to tumors of multifunctional paclitaxel/SPIO-loaded nanoparticles for tumor imaging and therapy. Journal of controlled release : official journal of the Controlled Release Society 2014, 194, 82–91, doi:10.1016/j.jconrel.2014.07.059. [PubMed: 25178270]
42. Závišová V; Koneracká M; Múčková M; Kopčanský P; Tomašovičová N; Lancz G; Timko M; Pätoprstá B; Bartoš P; Fabián M Synthesis and characterization of polymeric nanospheres loaded with the anticancer drug paclitaxel and magnetic particles. Journal of Magnetism and Magnetic Materials 2009, 321, 1613–1616, doi:10.1016/j.jmmm.2009.02.097.
43. Massart R Preparation of aqueous magnetic liquids in alkaline and acidic media. IEEE Transactions on Magnetics 1981, 17, 1247–1248, doi:10.1109/TMAG.1981.1061188.
44. Sun S; Zeng H Size-controlled synthesis of magnetite nanoparticles. J Am Chem Soc 2002, 124, 8204–8205, doi:10.1021/ja026501x. [PubMed: 12105897]
45. Onali P; Olianas MC; Gessa GL Characterization of dopamine receptors mediating inhibition of adenylate cyclase activity in rat striatum. Mol Pharmacol 1985, 28, 138–145. [PubMed: 2410769]
46. Si F; Ross GM; Shin SH Glutathione protects PC12 cells from ascorbate- and dopamine-induced apoptosis. Exp Brain Res 1998, 123, 263–268, doi:10.1007/s002210050568. [PubMed: 9860264]
47. Zhang J; Kravtsov V; Amarnath V; Picklo MJ; Graham DG; Montine TJ Enhancement of dopaminergic neurotoxicity by the mercapturate of dopamine: relevance to Parkinson's disease. J Neurochem 2000, 74, 970–978, doi:10.1046/j.1471-4159.2000.0740970.x. [PubMed: 10693927]
48. Lassenberger A; Bixner O; Gruenewald T; Lichtenegger H; Zirbs R; Reimhult E Evaluation of High-Yield Purification Methods on Monodisperse PEG-Grafted Iron Oxide Nanoparticles. Langmuir 2016, 32, 4259–4269, doi:10.1021/acs.langmuir.6b00919. [PubMed: 27046133]
49. Wu M; Zhang D; Zeng Y; Wu L; Liu X; Liu J Nanocluster of superparamagnetic iron oxide nanoparticles coated with poly (dopamine) for magnetic field-targeting, highly sensitive MRI and photothermal cancer therapy. Nanotechnology 2015, 26, 115102, doi:10.1088/0957-4484/26/11/115102. [PubMed: 25721867]
50. Teng W; Cappello J; Wu X Physical crosslinking modulates sustained drug release from recombinant silk-elastinlike protein polymer for ophthalmic applications. J Control Release 2011, 156, 186–194, doi:10.1016/j.jconrel.2011.07.036. [PubMed: 21839125]

51. Huang J; Zhong X; Wang L; Yang L; Mao H Improving the magnetic resonance imaging contrast and detection methods with engineered magnetic nanoparticles. Theranostics 2012, 2, 86–102, doi:10.7150/thno.4006. [PubMed: 22272222]
52. Ai H; Flask C; Weinberg B; Shuai X-T; Pagel MD; Farrell D; Duerk J; Gao J Magnetite-Loaded Polymeric Micelles as Ultrasensitive Magnetic-Resonance Probes. Advanced Materials 2005, 17, 1949–1952, doi:doi:10.1002/adma.200401904.
53. Berret JF; Schonbeck N; Gazeau F; El Kharrat D; Sandre O; Vacher A; Airiau M Controlled clustering of superparamagnetic nanoparticles using block copolymers: design of new contrast agents for magnetic resonance imaging. J Am Chem Soc 2006, 128, 1755–1761, doi:10.1021/ja0562999. [PubMed: 16448152]
54. Tromsdorf UI; Bigall NC; Kaul MG; Bruns OT; Nikolic MS; Mollwitz B; Sperling RA; Reimer R; Hohenberg H; Parak WJ; et al. Size and surface effects on the MRI relaxivity of manganese ferrite nanoparticle contrast agents. Nano Lett 2007, 7, 2422–2427, doi:10.1021/nl071099b. [PubMed: 17658761]
55. Zeng J; Jing L; Hou Y; Jiao M; Qiao R; Jia Q; Liu C; Fang F; Lei H; Gao M Anchoring Group Effects of Surface Ligands on Magnetic Properties of Fe3O4 Nanoparticles: Towards High Performance MRI Contrast Agents. Advanced Materials 2014, 26, 2694–2698, doi:10.1002/adma.201304744. [PubMed: 24615901]
56. Tong S; Hou S; Zheng Z; Zhou J; Bao G Coating optimization of superparamagnetic iron oxide nanoparticles for high T2 relaxivity. Nano Lett 2010, 10, 4607–4613, doi:10.1021/nl102623x. [PubMed: 20939602]
57. Najafian N; Shanehsazzadeh S; Hajesmaeelzadeh F; Lahooti A; Gruettner C; Oghabian MA Effect of Functional Group and Surface Charge of PEG and Dextran-Coated USPIO as a Contrast Agent in MRI on Relaxivity Constant. Applied Magnetic Resonance 2015, 46, 685–692, doi:10.1007/s00723-015-0667-2.
58. Khalkhali M; Rostamizadeh K; Sadighian S; Khoeini F; Naghibi M; Hamidi M The impact of polymer coatings on magnetite nanoparticles performance as MRI contrast agents: a comparative study. DARU Journal of Pharmaceutical Sciences 2015, 23, 45, doi:10.1186/s40199-015-0124-7. [PubMed: 26381740]
59. Lee N; Hyeon T Designed synthesis of uniformly sized iron oxide nanoparticles for efficient magnetic resonance imaging contrast agents. Chemical Society reviews 2012, 41, 2575–2589, doi:10.1039/c1cs15248c. [PubMed: 22138852]
60. Moore A; Marecos E; Bogdanov A Jr.; Weissleder R Tumoral distribution of long-circulating dextran-coated iron oxide nanoparticles in a rodent model. Radiology 2000, 214, 568–574, doi:10.1148/radiology.214.2.r00fe19568. [PubMed: 10671613]
61. Turetschek K; Roberts TP; Floyd E; Preda A; Novikov V; Shames DM; Carter WO; Brasch RC Tumor microvascular characterization using ultrasmall superparamagnetic iron oxide particles (USPIO) in an experimental breast cancer model. J Magn Reson Imaging 2001, 13, 882–888, doi:10.1002/jmri.1126. [PubMed: 11382948]
62. Daldrup-Link HE; Golovko D; Ruffell B; Denardo DG; Castaneda R; Ansari C; Rao J; Tikhomirov GA; Wendland MF; Corot C; et al. MRI of tumor-associated macrophages with clinically applicable iron oxide nanoparticles. Clinical cancer research : an official journal of the American Association for Cancer Research 2011, 17, 5695–5704, doi:10.1158/1078-0432.Ccr-10-3420. [PubMed: 21791632]
63. Klyachko NL; Sokolsky-Papkov M; Pothayee N; Efremova MV; Gulin DA; Pothayee N; Kuznetsov AA; Majouga AG; Riffle JS; Golovin YI; et al. Changing the enzyme reaction rate in magnetic nanosuspensions by a non-heating magnetic field. Angew Chem Int Ed Engl 2012, 51, 12016–12019, doi:10.1002/anie.201205905. [PubMed: 23081706]
64. Zhang E; Kircher MF; Koch M; Eliasson L; Goldberg SN; Renstrom E Dynamic magnetic fields remote-control apoptosis via nanoparticle rotation. ACS Nano 2014, 8, 3192–3201, doi:10.1021/nn406302j. [PubMed: 24597847]

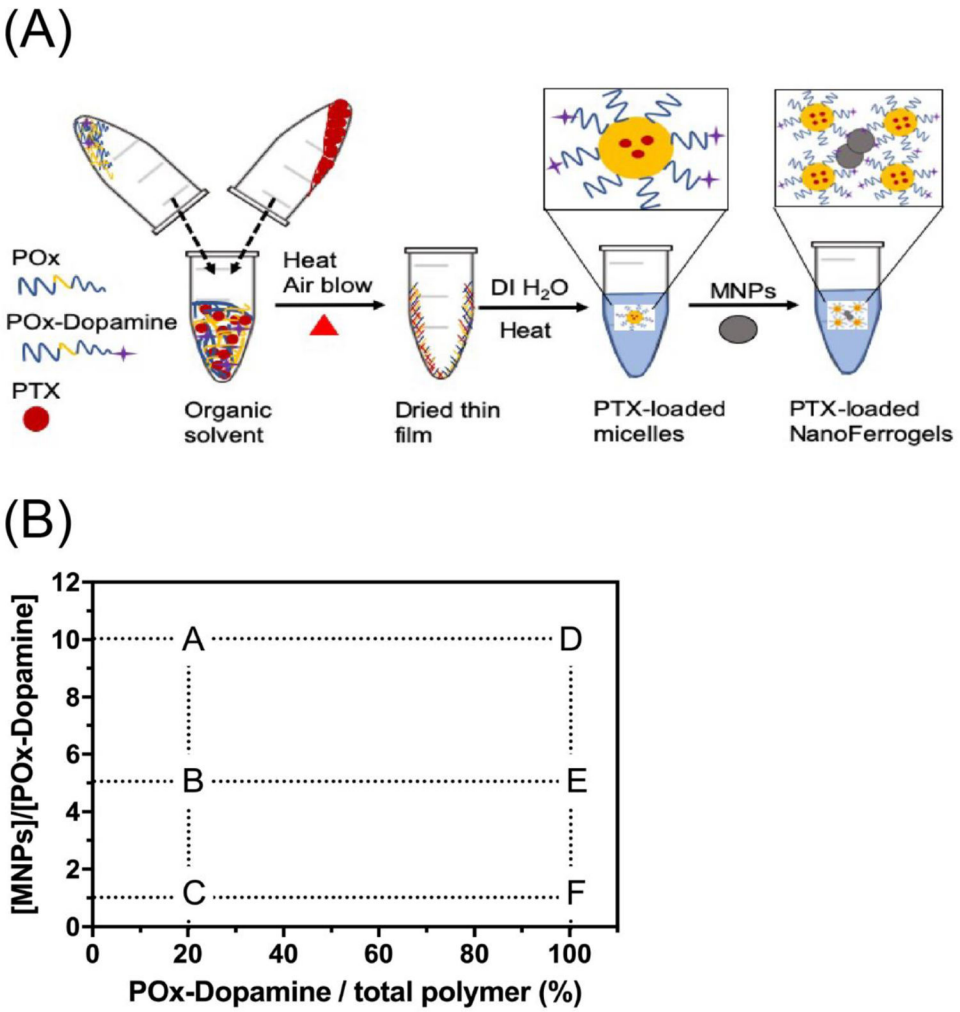

Fig. 1.

(A) Schematics of the preparation of PTX-NFGs and (B) summary of MNPs, POx-Dopamine and POx compositions in the blank NFGs and PTX-NFGs (see, also Table 1).

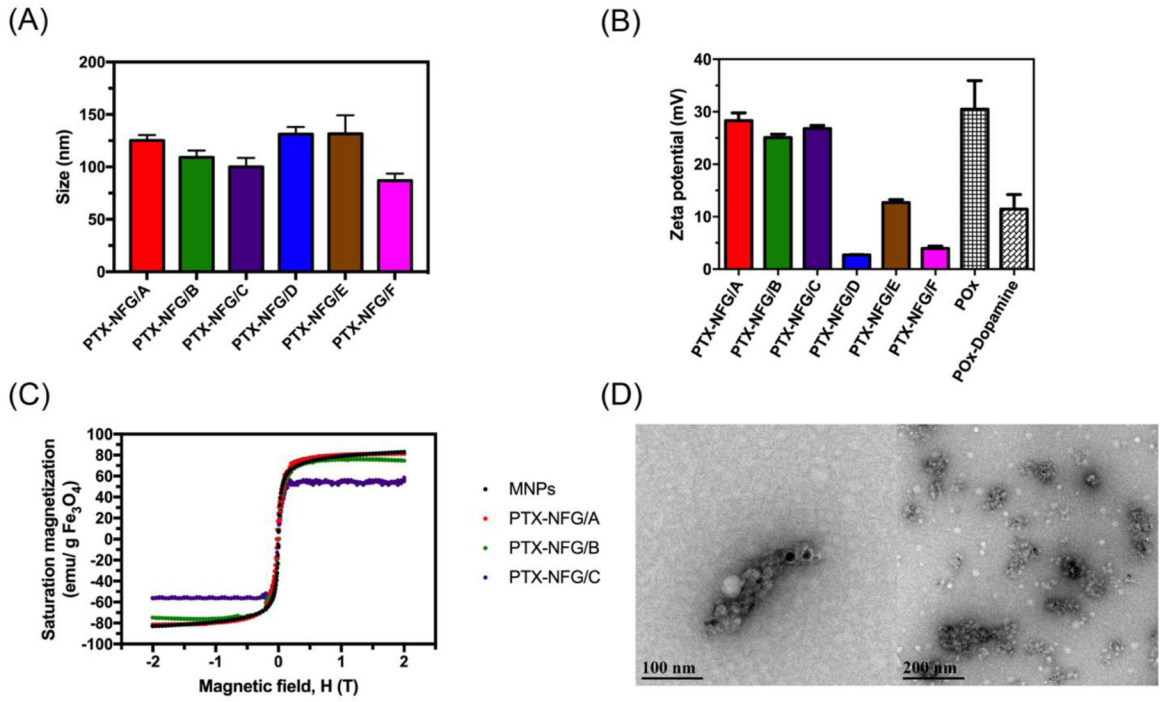

Fig. 2.

(A) Hydrodynamic diameter of PTX-NFGs dispersed in PBS, **(B)** zeta potential of PTX-NFGs, POx micelles, and POx-Dopamine micelles, **(C)** saturation magnetization of PTX-NFGs and **(D)** Representative PTX-NFGs TEM image (PTX-NFG/B). Data are mean ± S.D.

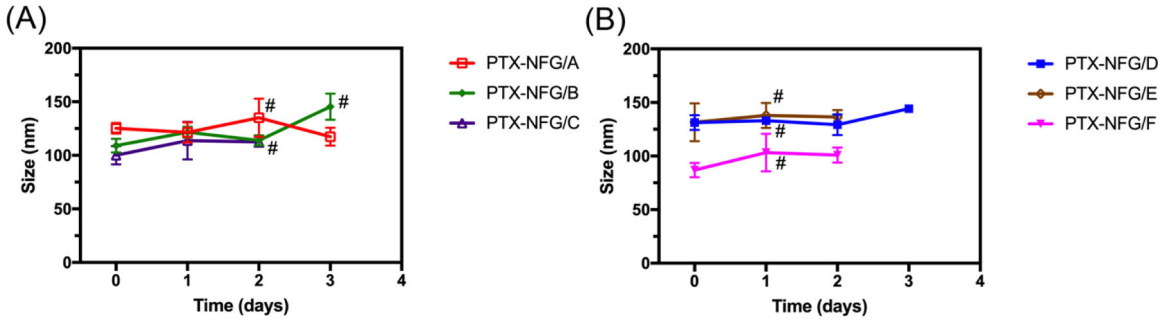

Fig. 3.

Colloidal stability of PTX-NFGs prepared with **(A)** 20% POx-Dopamine (PTX-NFG/A-C) and **(B)** 100% POx-Dopamine (PTX-NFG/D-F). The samples (1 mg mL^{-1}) were incubated in PBS over period of 3 days. Data represented mean ± SD (n=3). # indicate precipitation.

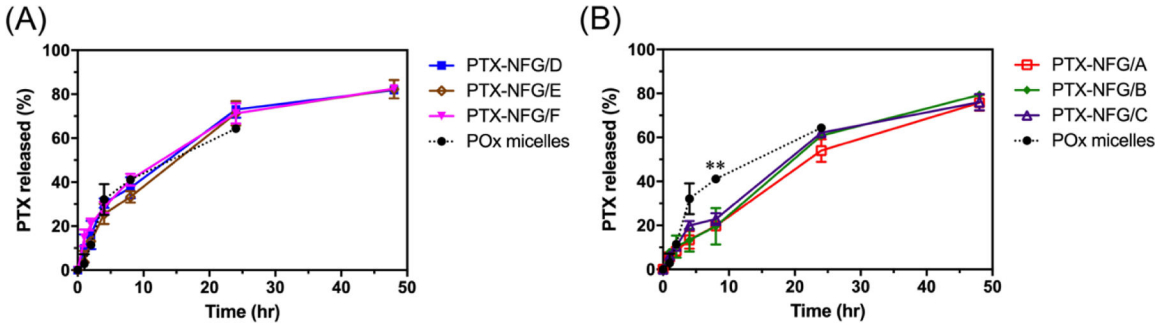

Fig. 4.

A cumulative PTX release from PTX-NFGs at 37 °C in the presence of 40 g L^{-1} of BSA. PTX release comparison between POx micelles and **(A)** PTX-NFGs/D-F, **(B)** PTX-NFGs/A-C Data are mean ± SD (n=3, *P<0.05, **P<0.01).

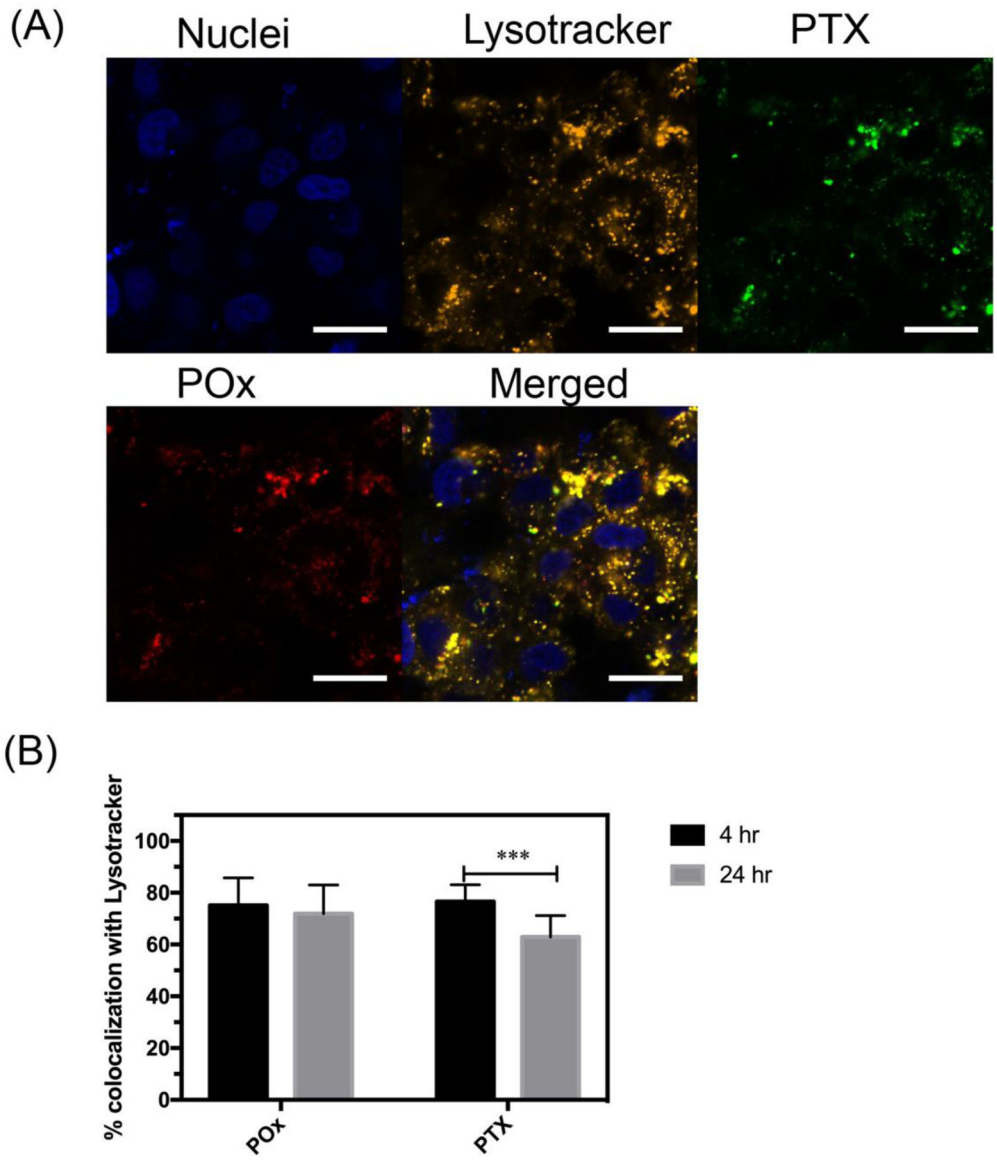

Fig. 5.

(A) Intracellular distribution of fluorescently labeled PTX-NFG/B in MCF-7 breast cancer cells after 4 h of incubation (bar = 20 μm). **(B)** Quantification of the colocalization of AF647-POx (red) and OG488-PTX (green) with lysosomes (orange) as determined by ImageJ software after 4 and 24 h of incubation (***P<0.001). Nuclei were stained with Hoechst 33342 (blue).

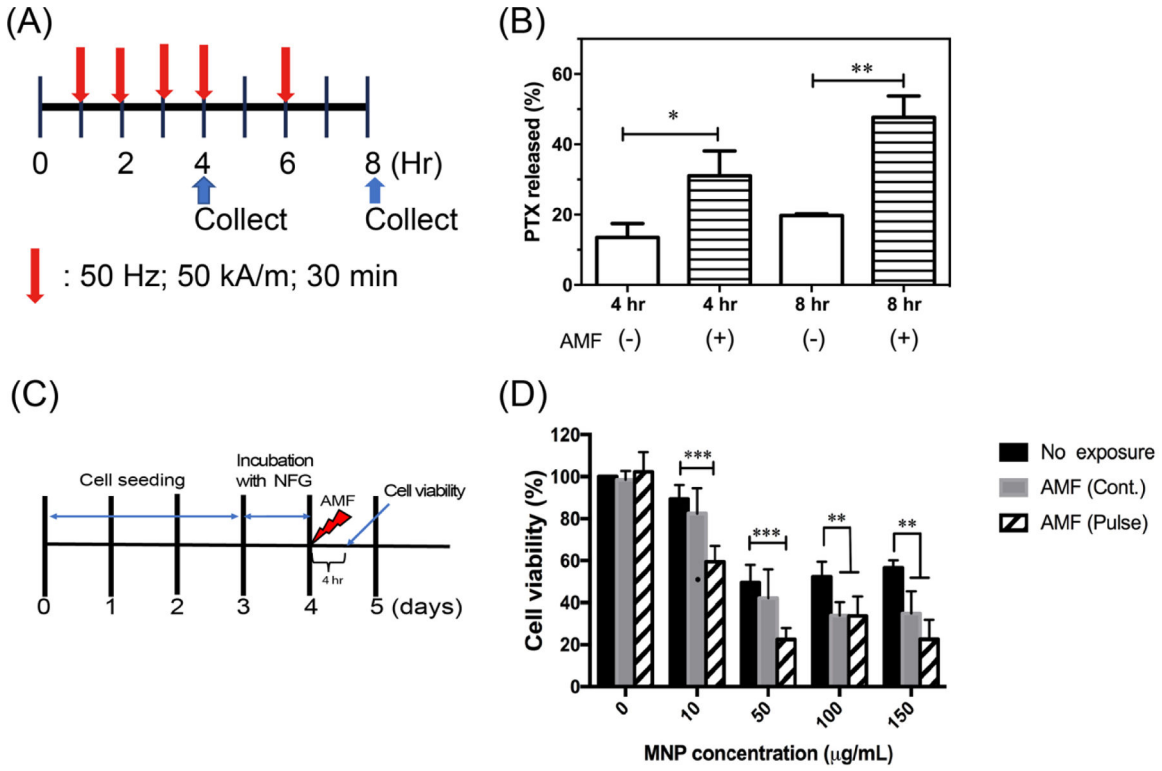

Fig. 6.

Remote magneto-mechanical actuation of PTX-NFG and NFG in AC magnetic field. **(A)** A scheme illustrating the exposure and PTX release measurement timeline. Red arrow indicates application of AC magnetic field (50 kA/m, 50 Hz) either continuous or pulse for 30 min. **(B)** The effect of the AC magnetic field exposure on the release of PTX from PTX-NFG/B at 4 h, and 8 h (n=3). **(C)** A scheme illustrating the exposure and cell viability measurement timeline. Red arrow indicates times of application of AC magnetic field. **(D)** Cell viability of LCC-6-WT cancer cells following exposure to continuous (gray) or pulsed (striped) AC magnetic field. **P<0.01; ***P<0.001 compared to no exposure. Data are mean ± S.D. (n=6).

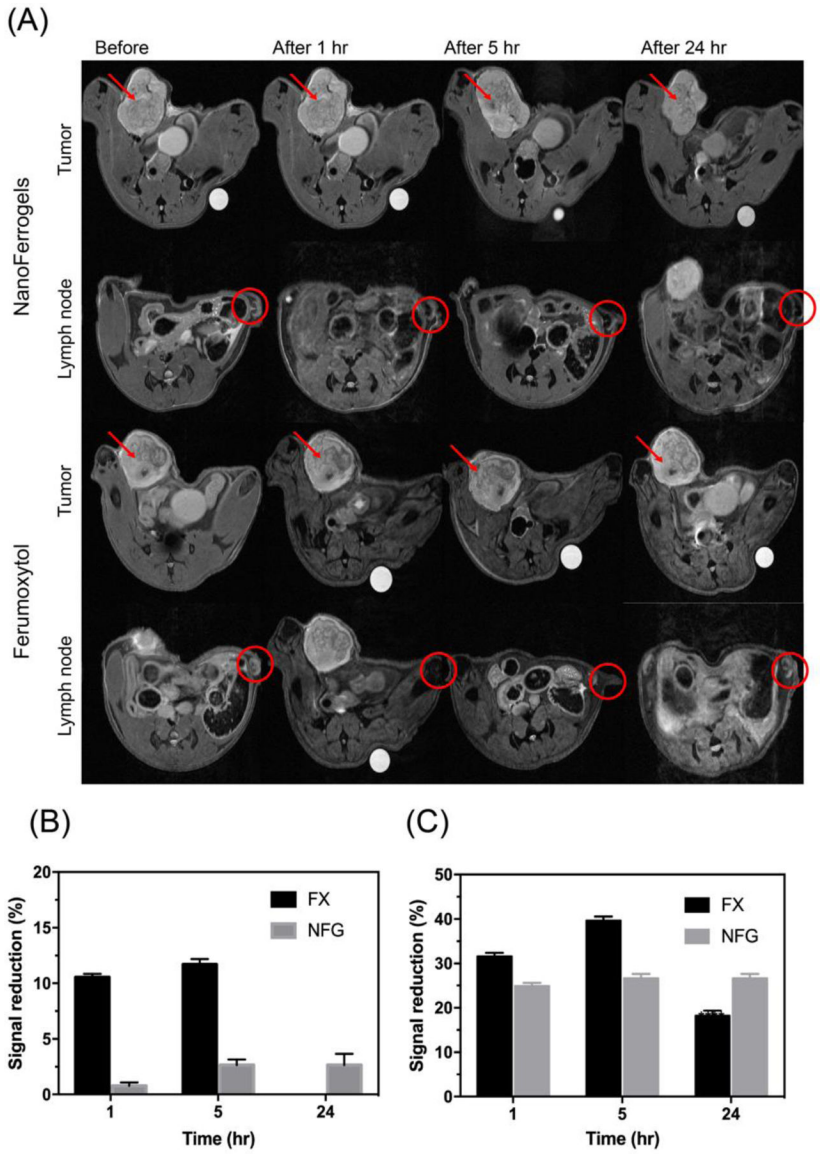

Fig. 7.

(A) T_2-weighted images obtained from tumor and lymph node at different time points after NFG/E or Ferumoxytol (FX) administration. Red arrow and circle indicated the tumor tissue and lymph node, respectively. **(B)** Signal reduction percentage of NFG/E and Ferumoxytol compared to reference in tumor. **(C)** Signal reduction percentage of NFG/E and Ferumoxytol compared to reference in lymph node. Data represented mean ± S.D. (n=3).

Table 1.

Composition and loading characteristics of PTX-NFGs

Formulation	MNP: POx-Dopamine ratio	Feeding amount (mg)				Loading Efficiency (LE)[1] (%)		Loading capacity (LC)[2] (%)	
		POx	POx-Dopamine	PTX	MNPs	PTX	MNPs	PTX	MNPs
PTX-NFG/A	1:4	8	2	2	0.5	106.9	67.5	17.1	2.7
PTX-NFG/B	1:8	8	2	2	0.24	88.2	68.8	14.4	1.2
PTX-NFG/C	1:40	8	2	2	0.05	95.8	72.3	15.9	0.3
PTX-NFG/D	1:4	0	10	2	2.4	97.9	69.0	13.5	11.9
PTX-NFG/E	1:8	0	10	2	1.2	100.0	71.0	15.1	6.7
PTX-NFG/F	1:40	0	10	2	0.24	102.3	63.7	16.7	1.3

[1] LE (wt. %) of either PTX (or MNPs) was calculated as the amount of PTX (or MNP) in final formulation/the feed amount of PTX (or MNP) X100.

[2] LC (wt %) for either PTX or MNPs was calculated as the amount of PTX or MNPs in final formulation X100 / the amount of dispersed phase in the formulation.

Table 2.

Saturation magnetization of PTX-NFGs

Sample	MNP:POx-Dopamine ratio	Saturation magnetization (emu/g Fe_3O_4)	Fraction of saturation magnetization of Fe_3O_4 (%)
Fe_3O_4	n/a	82.9	100
PTX-NFG/A	1:4	81.3	98.0
PTX-NFG/D	1:4	78.1	94.2
PTX-NFG/B	1:8	74.7	90.1
PTX-NFG/E	1:8	77.2	93.1
PTX-NFG/C	1:40	56.2	67.8
PTX-NFG/F	1:40	55.0	66.3

Table 3.

IC_{50} values of the various PTX-NFGs in breast cancer cell lines.

Treatment	IC_{50} (ng/mL)[a]		
	MCF-7	LCC-6-WT	LCC-6-MDR
PTX	4.2 ± 2.7	6.6 ± 2.1	217 ± 76
PTX-NFG/A	9.2 ± 2.8	7.5 ± 1.1	102 ± 14**
PTX-NFG/B	4.7 ± 1.9	6.2 ± 2.2	399 ± 202
PTX-NFG/C	5.2 ± 4.4	15.8 ± 2.7	245 ± 50
PTX-NFG/D	8.1 ± 7.7	4.2 ± 0.3	63 ± 22**
PTX-NFG/E	2.0 ± 1.5	5.3 ± 1.1	89 ± 37**
PTX-NFG/F	5.8 ± 1.3	1.7 ± 0.8	243 ± 24

[a]Data represent mean ± S.D. (n=6).

**P<0.01 compared to free PTX.

Table 4.

Transverse relaxivity (r_2) of PTX-NFGs.

Formulation	MNP : POx-Dopamine ratio	POx-Dopamine content vs total POx (%)	MNPs content (%)	r_2 ($s^{-1}mM^{-1}$)
PTX-NFG/A	1:4	20	2.7	30.3 ± 0.8
PTX-NFG/B	1:8	20	1.2	18.8 ± 2.6
PTX-NFG/C	1:40	20	0.3	16.0 ± 0.2
PTX-NFG/D	1:4	100	11.9	22.0 ± 2.4
PTX-NFG/E	1:8	100	6.7	15.3 ± 0.5
PTX-NFG/F	1:40	100	1.3	13.8 ± 0.3